Estimation of the fractions of luminescence of water at higher energy than Cerenkov-light threshold for various types of radiation

Yoshiyuki Hirano
Seiichi Yamamoto

SPIE.

Estimation of the fractions of luminescence of water at higher energy than Cerenkov-light threshold for various types of radiation

Yoshiyuki Hirano and Seiichi Yamamoto*
Nagoya University Graduate School of Medicine, Department of Radiological and Medical Laboratory Sciences, Nagoya, Japan

Abstract. Although the luminescence of water at a lower energy than the Cerenkov-light (CL) threshold has been found for various types of radiation, the fractions of the luminescence of water to the total produced light have not been obvious for radiations at a higher energy than the CL threshold because it is difficult to separate these two types of light. Thus, we used a Monte Carlo simulation to estimate the fractions of the luminescence of water for various types of radiation at a higher energy than the CL threshold to confirm the major component of the produced light. After we confirmed that the estimated light production of the luminescence of water could adequately simulate the experimental results, we calculated the produced light photons of this luminescence and the CL from water for protons (170 MeV), carbon ions (330 MeV/n), high-energy x-ray (6 MV) from a linear accelerator (LINAC), high-energy electrons (9 MeV) from LINAC, positrons (F-18, C-11, O-15, and N-13), and high-energy gamma photon radionuclides (Co-60). For protons, the major fraction of the produced light was the luminescence of water in addition to the CL from the prompt gamma photons produced by the nuclear interactions. For carbon ions, the major fraction of the produced light was the luminescence of water and the CL produced by the secondary electrons in addition to the prompt gamma photons produced by the nuclear interactions. For high-energy x-ray and electrons from LINAC, the fractions of luminescence of water were ∼0.1% to 0.2%. The fractions of luminescence of water for positrons were 0.2% to 1.5% and that for Co-60 was 0.4%. We conclude that the major fractions of light produced from x-ray and electrons from LINAC, positron radionuclides, and the Co-60 source are CL, with fractions of the luminescence of water from <0.1% to 1.5%. © *The Authors. Published by SPIE under a Creative Commons Attribution 4.0 Unported License. Distribution or reproduction of this work in whole or in part requires full attribution of the original publication, including its DOI.* [DOI: 10.1117/1.JBO.24.6.066005]

Key words: luminescence of water; Cerenkov light; proton, carbon ion; linear accelerator; positrons; Monte Carlo simulation.

Paper 190044R received Mar. 2, 2019; accepted for publication May 21, 2019; published online Jun. 19, 2019.

1 Introduction

Cerenkov light (CL) imaging is a relatively new technology that detects visible photons from a high-speed electron-induced light with a high-sensitivity optical camera used for dose estimation of a medical linear accelerator (LINAC)[1–9] and molecular imaging using positron radionuclides.[10–18] Because CL is emitted above the threshold energy of the electrons or positrons (∼260 keV)[19] and other optical light is not known for water at a lower energy than the CL threshold, the optical light emitted from water at a higher energy than the CL is believed to be composed of only CL.

Recently, we found the luminescence of water at a lower energy than the CL threshold for protons,[20] carbon ions,[21] alpha particles,[22] beta particles,[23] and low-energy x-ray.[24] The luminescence of water at a lower energy than the CL threshold has linearity to energy[25] and shows a distribution that is identical to the dose in protons.[26] We also found that the optical photon production of the luminescence of water is ∼0.1 photons/MeV, by comparing the experimental results with those of the simulation.[27] These findings suggest that the optical light emitted by the irradiation of various radiations or radionuclides contain some luminescence of water in the light,

even at a higher energy than the CL threshold. In some cases, the term "CL" or "CL imaging" might not be appropriate if the optical light were mainly from the luminescence of water. In fact, there has been a misunderstanding in that the scintillation of optical fiber was recognized as CL,[28] even though the proton energy is lower than the CL threshold, as pointed out by Darafsheh et al.[29]

Clarifying the major components of the types of optical light during irradiation of various radiations at a higher energy than the CL is important, to avoid confusion about the sources of light. However, the separation of the luminescence of water and CL is difficult to achieve by experiment because the light spectra of these two are similar.[30] Furthermore, because the temporal response of the luminescence of water is thought to be the same as that of CL,[30] the separation of these two types of light with a triggering-synchronized camera employed for molecular probe imaging[31] would also be difficult. Monte Carlo simulation is a possible method to separately calculate the intensities of these two types of light if we incorporate the process of the luminescence of water in this simulation.[27] Thus, we have used Monte Carlo simulation to estimate the fractions of the luminescence of water for various types of radiations and radionuclides that emit radiation with a higher energy than the CL threshold as a way to clarify the major components of the produced light.

*Address all correspondence to Seiichi Yamamoto, E-mail: s-yama@met .nagoya-u.ac.jp

2 Materials and Methods

2.1 Simulation for Luminescence of Water and Cerenkov-light

First, we investigated whether the light production of the luminescence of water measured by experiments could be accurately represented by the Monte Carlo simulation that we used. Then, using the Monte Carlo simulation, we calculated the produced light photons of the luminescence of water and CL for protons (170 MeV), carbon ions (330 MeV/n), high-energy x-ray (6 MV) from a LINAC, high-energy electrons (9 MeV) from LINAC, major positron radionuclides (F-18, C-11, O-15, and N-13), and high-energy gamma photon radionuclides (Co-60).

2.1.1 Monte Carlo simulation software

We used Geant4 (version 10.4)[32] for the Monte Carlo simulation because it is used in many fields and its quality has been evaluated extensively. Moreover, it includes the optical photon processes (G4OpticalProcess), CL (G4Cerenkov), and scintillation photon generation (G4Scintillation) in the software class. For light production from the luminescence of water at a lower energy than the CL threshold, we used the scintillation photon-generation process in the software.[32] For the CL-generation process, we separately calculated the fractions from the prompt gamma photons and the secondary electrons produced by the primary beam if the energy of the secondary electrons was higher than the CL threshold. We did not include the CL from the positrons produced by the nuclear reactions because it is dependent on the acquisition time. In addition, it is relatively a minor process compared to the other light-emitting processes.[20]

To simulate the optical processes, light photons of 0.1 photons/MeV were used for the luminescence of water.[27] For the refractive index of water and the spectrum of the luminescence of water in the simulation, we used the same values used in the previous work.[27] The wavelength of optical photons was simulated between 200 and 800 nm.

In this simulation, we scored the position of the optical photons generated in water, the emission angle, the wavelength, the creator process name used to discriminate between the Cerenkov and scintillation processes, and the parent particle name. In the Cerenkov process, since the parent particle of an optical photon was nearly an electron, we recorded it as the parent of the electron. In all simulations, we used the G4HadronPhysicsQGSP_BERT for the hadronic processes and G4EmStandardPhysics_option3 for the electromagnetic processes. The production cut range of secondary particles (photons, electrons, positrons, and protons) in this simulation was set to 0.1 mm.

2.1.2 Confirmation of the Monte Carlo simulation's accuracy

To confirm the accuracy of the Monte Carlo simulation, we compared the depth profiles of the measured data of protons and carbon ions with those obtained by the simulation.

The experimental setup is shown schematically in Fig. 1. A transparent container as a phantom was filled with water, and a cooled CCD camera (BITRAN BS-40L, Japan) with a C-mount F-1.4 lens (focal length: 8 mm) was set 40 cm from the phantom's water surface. The proton energy irradiated to water was 100 MeV, and the carbon-ion energy irradiated to water was
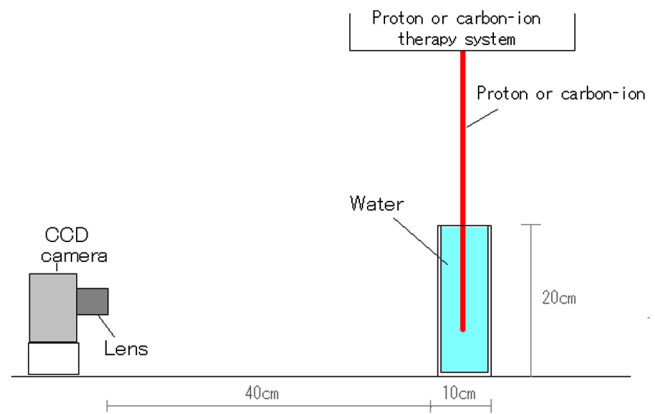
Fig. 1 Schematic drawing of luminescence imaging and simulation during proton or carbon-ion irradiation to confirm the Monte Carlo simulation's accuracy.

240 MeV/u. The water phantom's dimensions were 20 cm (horizontal) × 20 cm (vertical) × 10 cm (width).[20,21] The beam sizes of the protons and carbon ions used for the experiments were 23 mm FWHM and 17 mm FWHM, respectively.

We irradiated protons or carbon ions to the water phantom and measured the luminescence image (luminescence and CL) of water with the CCD camera. The source-to-surface distance (SSD) for proton and carbon-ion experiments was 1 m. For simulation of proton, carbon ion, LINAC x-ray, and LINAC electrons, the SSD was also 1 m. In the simulation, we used the same geometrical configuration and protons or carbon ions were irradiated to the phantom. Then, we compared the depth profiles between the measured and the simulated profiles.

On both experimental and simulated images, we set the profiles along the images of the beams and calculated the depth profiles from the intensities of the images. We then compared the shapes of the depth profiles.

2.1.3 Calculation of the fractions of the luminescence of water to the total produced light for various types of radiation by Monte Carlo simulation

We calculated the luminescence of water and CL for various types of radiation by Monte Carlo simulation. These included protons, carbon ions, x-ray from LINAC, electrons from LINAC, major positron radionuclides, and high-energy gamma photon radionuclides. The same Monte Carlo simulation was used as that whose accuracy had been confirmed.

Figure 2(a) is a schematic drawing of the simulation of luminescence and CL for irradiations of protons, carbon ions, x-ray from LINAC, and electrons from LINAC. Each of these radiations was irradiated to the water phantom, and the produced luminescence and CL were measured from the side of the beam direction. The dimensions of the water phantom used were 30 cm (horizontal) × 30 cm (vertical) × 30 cm (width). A larger phantom than in the experiments was used for the simulation because we evaluated the light produced for the higher-energy radiations of protons and carbon ions, which had longer ranges.

Figure 2(b) is a schematic drawing of the simulation of luminescence and CL for positrons and high-energy gamma sources. Point sources were used for the simulation. One of these sources was positioned at the center of the water phantom, and the produced luminescence and CL were measured from the side of the beam direction. The dimensions of the water phantom used were 30 cm (horizontal) × 30 cm (vertical) × 30 cm (width).
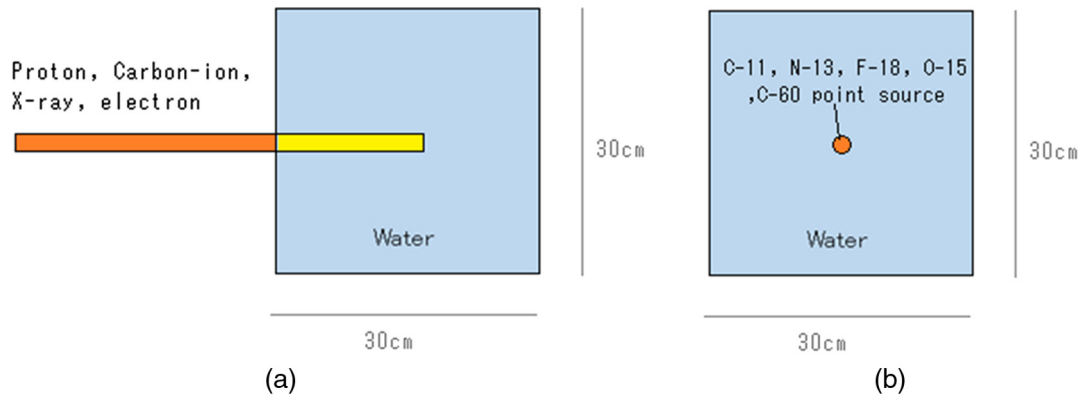
Fig. 2 Schematic drawing of the simulation of luminescence and CL (a) for protons, carbon ions, x-ray from LINAC, and electrons from LINAC and (b) that for positrons and high-energy gamma sources.

The spatial resolution of the simulated images was 1 mm. We also calculated the images of the light photons emitted to the side of the beam direction. The profiles estimated for the simulated images were summed for the entire area of the image (30 × 30 cm) along with the beam direction.

Calculation of the fraction of the luminescence of water for protons by Monte Carlo simulation. We calculated the fraction of the luminescence of water to the total produced light for 170 MeV protons. This proton energy was selected because it was higher than the CL threshold for the secondary electrons produced by the protons and thus adequate to observe the CL from protons. The beam of the proton used for the simulation was ideal pencil beam with the size of <1 mm. We calculated the number of light photons produced by the luminescence of water, the CL from the secondary electrons produced by the protons, and the CL from the electrons produced by the prompt gamma photons.

To derive the depth profiles for the luminescence of water, the CL from the secondary electrons produced by protons, and the CL from the electrons produced by the prompt gamma photons, we summed all of the light photons in the image for each different type of light and plotted each profile as a function of depth.

Calculation of the fraction of the luminescence of water for carbon ions by Monte Carlo simulation. We calculated the fraction of the luminescence of water to the total produced light for 330-MeV/u protons because the energy was higher than that used for the comparison in the experiment. The beam size of the carbon ion used for the simulation was ideal pencil beam with the size of <1 mm. We calculated the number of light photons produced by the luminescence of water, the CL from the secondary electrons produced by carbon ions, and the CL from the electrons produced by the prompt gamma photons. The same image processing used for protons was also used for the simulated carbon-ion image.

Calculation of the fraction of the luminescence of water for LINAC x-ray by Monte Carlo simulation. We calculated the fraction of the luminescence of water to the total produced light for 6-MV x-ray from LINAC because it was a typical energy used for photon therapy. The size of the beam was 100 mm × 100 mm. We calculated the number of light photons produced by the luminescence of water and the CL from the

electrons produced by x-ray. For the x-ray energy distribution from LINAC, we used the IAEA phase space data.

To derive the depth profiles for the luminescence of water and the CL from the secondary electrons produced by x-ray, we summed all of the light photons in the image for these two types of light and plotted the profiles as a function of depth.

Calculation of the fraction of the luminescence of water for LINAC electrons by Monte Carlo simulation. We calculated the fraction of the luminescence of water to the total produced light for 9-MeV x-ray from a LINAC because it was a typical energy used for electron therapy. The size of the beam was 100 mm × 100 mm. We calculated the number of light photons produced by the luminescence of water and the CL produced by the irradiated electrons. No applicator was used for the beam. For the electrons and scattered x-ray from LINAC, we used the IAEA phase space data.

To derive the depth profiles for the luminescence of water, the CL from the electrons, and the CL from the secondary electrons produced by Bremsstrahlung x-ray, we summed all of the light photons in the image for these three types of light and plotted the profiles as a function of depth.

Calculation of the fractions of the luminescence of water for positron sources by Monte Carlo simulation. We calculated the fractions of the luminescence of water to the total produced light for major positron radionuclides from positron emission tomography (PET) studies. These were F-18 (maximum positron energy: 0.64 MeV), C-11 (maximum positron energy: 0.96 MeV), O-15 (maximum positron energy: 1.70 MeV), and N-13 (maximum positron energy: 1.19 MeV). We calculated the number of light photons from the luminescence of water, the CL from positrons, and the CL from the electrons produced by annihilation gamma photons (511 keV) emitted from positrons. The positron source was the ideal point source with a size of <1 mm and was located at the center of the phantom.

To derive the horizontal profiles for the luminescence of water, the CL from positrons, and the CL from 511-keV gamma photons, we summed all of the light photons in the image for these three types of light and plotted the profiles in the horizontal direction.

Calculation of the fraction of the luminescence of water for high-energy gamma photon source by Monte Carlo simulation. We calculated the fraction of the luminescence

of water to the total produced light for a Co-60 gamma source (1.17 and 1.33 MeV) because it is often used for gamma irradiation of materials and the CL can be easily observed in a water pool for a Co-60 source with high activity. We calculated the number of light photons produced by the luminescence of water and the CL from the electrons produced by Co-60 gamma photons.

To derive the horizontal profiles for the luminescence of water and the CL from the secondary electrons of gamma photons, we summed all of the light photons in the image for these two types of light and plotted the profiles in the horizontal direction.

3 Results

3.1 Simulated Depth Profiles for Luminescence and Cerenkov Light

3.1.1 Confirmation of the Monte Carlo simulation's accuracy

The depth profiles of the experiment and the simulation for 100-MeV protons are shown in Fig. 3(a). As shown in the ratio

curve of the measured to simulated profiles in Fig. 3(b), these two curves were almost identical, with an average difference of 1.3% (minimum: −7% to maximum: +14%) between the water surface and the Bragg peak, although some difference was observed in the distribution probably due mainly to the statistical valuations of the profiles. These errors are acceptable compared with other luminescence production fractions of water.[27]

We also show the depth profiles of the experiment and the simulation for 240-MeV/u carbon ions in Fig. 3(c). As shown in the ratio curve of the measured to simulated profiles in Fig. 3(d), these two curves were also nearly identical, with an average difference of 1.8% (minimum: −8% to maximum: +9%) between the water surface and the Bragg peak, although there is some difference between the two curves, probably due to the parallax error for the experimental image. These errors are also acceptable compared with other luminescence production fractions of water.[27]

With these data, we confirmed that the simulation we used could produce reliable light distributions when light photons of 0.1 photons/MeV were used in the simulation of the luminescence of water for radiations at a higher energy than the CL threshold.
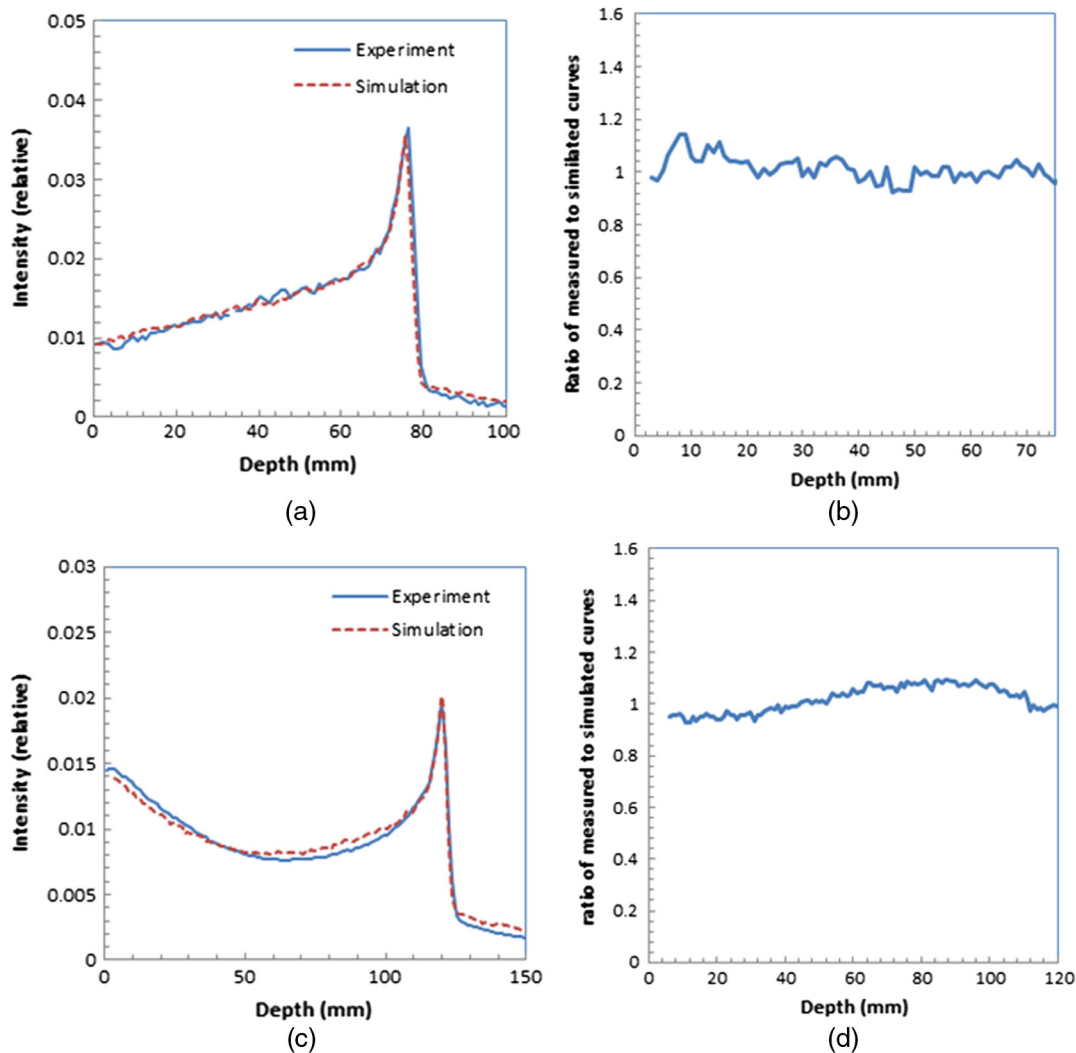
Fig. 3 Comparison of depth profiles of experiment and simulation for (a) 100-MeV protons, (b) ratio curve of measured to simulated curves for protons, (c) comparison of depth profiles of 240-MeV carbon ions, and (d) ratio curve of measured to simulated curves for carbon ions.

3.1.2 Calculation of the fractions of the luminescence of water to the total produced light for various types of radiations by Monte Carlo simulation

Calculation of the fraction of the luminescence of water for protons by Monte Carlo simulation. We show the simulated image and depth profiles of the luminescence and CL by simulation for 170-MeV protons in Figs. 4(a) and 4(b), respectively. The proton was irradiated from the left side of the image. In the depth profile, a broad distribution of the CL from the prompt gamma photon was observed with the luminescence of water, which was identical to the dose distribution. The CL from the prompt gamma photon was relatively large, at 33% of total light photons in the depth profile, because it was broadly distributed in the image. The CL from the secondary electrons of proton was observed in the shallow part of the distribution, but the fraction was small at only 0.4% of the total light. The fraction of the luminescence of water was very close to that of the CL.

Calculation of the fraction of the luminescence of water for carbon ions by Monte Carlo simulation. We show the simulated image and depth profiles of the luminescence and CL by simulation for 330-MeV/u carbon ions in Figs. 5(a) and 5(b), respectively. The carbon ion was irradiated from the left side of the image. A broad distribution of the CL from the prompt gamma photon was observed with the luminescence of water, which was identical to dose distribution. The CL from the prompt gamma photon was large at 37% of total light photons in the depth profile. The CL from the secondary electrons of the carbon ion was observed in the shallow part of the distribution. The fraction of the luminescence of water was nearly the same or slightly smaller than those of the CL.

Calculation of the fraction of the luminescence of water for x-ray from LINAC by Monte Carlo simulation. We show the image and the depth profiles of the luminescence and CL by simulation for 6-MV x-ray from LINAC in Figs. 6(a) and 6(b), respectively. In the depth profiles, the intensity of CL was much higher than that of the luminescence of water, where 99.8% of the total light was CL.

Calculation of the fraction of the luminescence of water for electrons from LINAC by Monte Carlo simulation. We show the image and the depth profiles of the luminescence and CL by simulation for 9-MeV electrons from LINAC in Figs. 7(a) and 7(b), respectively. In the depth profiles, the intensity of CL was much higher than that of the luminescence of water, where 99.9% of the total light was CL.

Calculation of the fractions of the luminescence of water for positrons by Monte Carlo simulation. We show the simulated depth profiles of luminescence and CL for the point sources of F-18, C-11, O-15, and N-13 in water in Figs. 8(a)–8(d), respectively. The intensities of CL from positrons were much higher than those of the luminescence of water. The intensity of CL of positrons was 92.4% to 98.2% of the total light.

The CL from annihilation photons was also higher than those of the luminescence of water. The intensity of CL of annihilation photons (511 keV) was 1.6% to 6.1% of the total light, which was higher than the luminescence of water (0.2% to 1.5% of total light).

Calculation of the fractions of the luminescence of water for high-energy gamma photon sources by Monte Carlo simulation. We show the simulated depth profiles of luminescence and CL for the point source of Co-60 in water in Fig. 9. The intensity of CL was much higher than that of the luminescence of water. The intensity of CL of Co-60 was 99.6% of the total light.

Summary of the simulation. We summarize the luminescence and CL fractions calculated by Monte Carlo simulation in all emitted light for protons, carbon ions, x-ray from LINAC, and electrons from LINAC in Table 1. For protons and carbon ions, the luminescence of water was one of the major

(a)   (b)
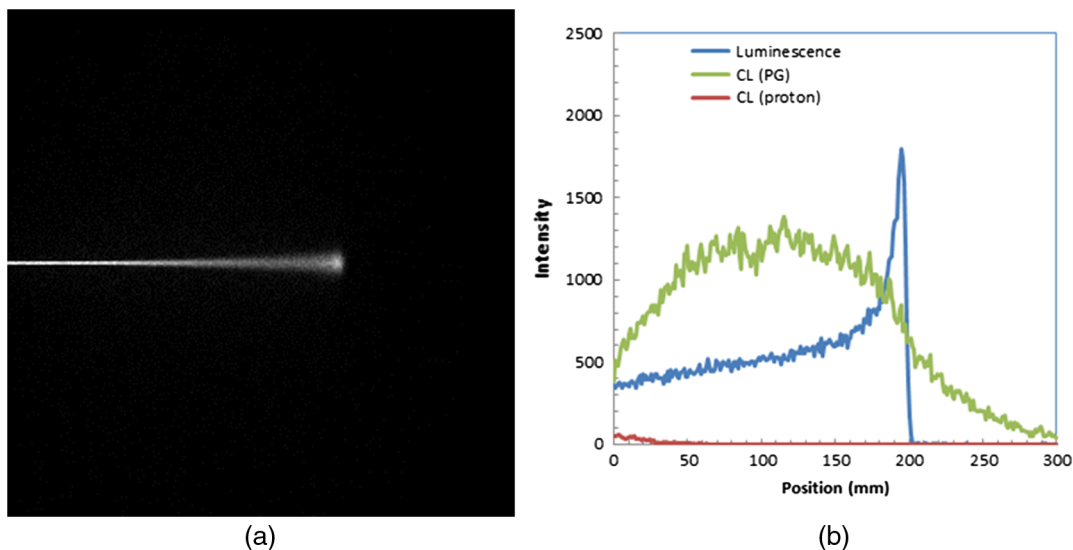
Fig. 4 (a) Simulated image and depth profiles of luminescence and CL for 170-MeV protons calculated by Monte Carlo simulation.
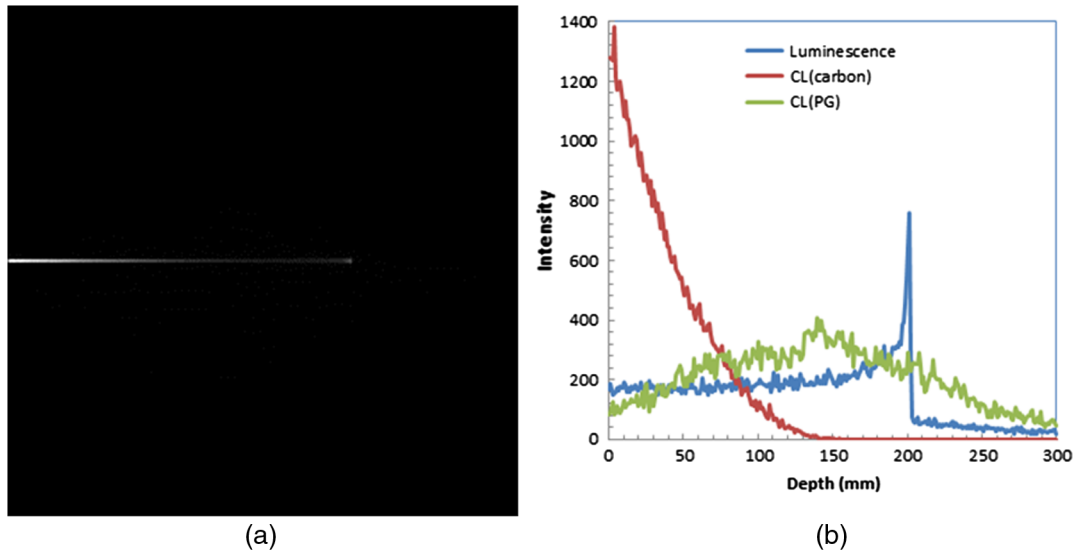
Fig. 5 (a) Simulated image and (b) depth profiles of luminescence and CL for 330-MeV/n carbon ions calculated by Monte Carlo simulation.
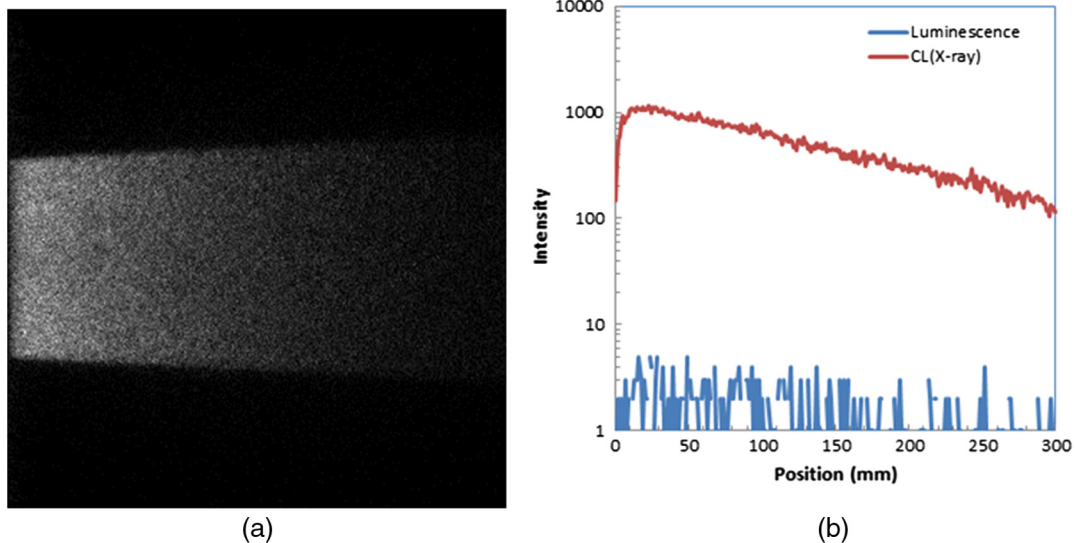
Fig. 6 (a) Simulated image and (b) depth profiles of luminescence and CL for 6-MV x-ray from LINAC calculated by Monte Carlo simulation.

components. However, the luminescence of water was only 0.1% to 0.2% for x-ray and electrons from LINAC.

We summarize the luminescence and CL fractions in all emitted light for positrons and Co-60 point sources in Table 2. The luminescence of water was a small component for light produced by positrons and Co-60 point sources. The fraction of light intensity of the luminescence of water was <0.2% to 1.5% of that of CL for the positrons and high-energy gamma photons.

4 Discussion

We could successfully calculate the images and profiles of the luminescence of water and CL for various types of radiations, and the fractions of the luminescence of water could be estimated. From our simulation results, it was obvious that the

fractions of the luminescence of water in the optical images for LINAC x-ray and electrons were small compared with those of CL. The fractions of the CL were 99.8% to 99.9% of the total light photons.

Furthermore, it became obvious that the fractions of the luminescence of water in the optical images for positrons were small compared with those of CL. The fractions of the CL were 98.5% to 99.9% of the total light photons for the optical light from positrons (F-18, C-11, O-15, and N-13), in addition to the high-energy gamma photon emitter (Co-60).

However, the intensities of the luminescence of water were comparable with those of the CL from the prompt gamma photons for protons and carbon ions. In the images, the luminescence of water was located in the beam position, while the CL from the prompt gamma photons was blurred. Consequently, the
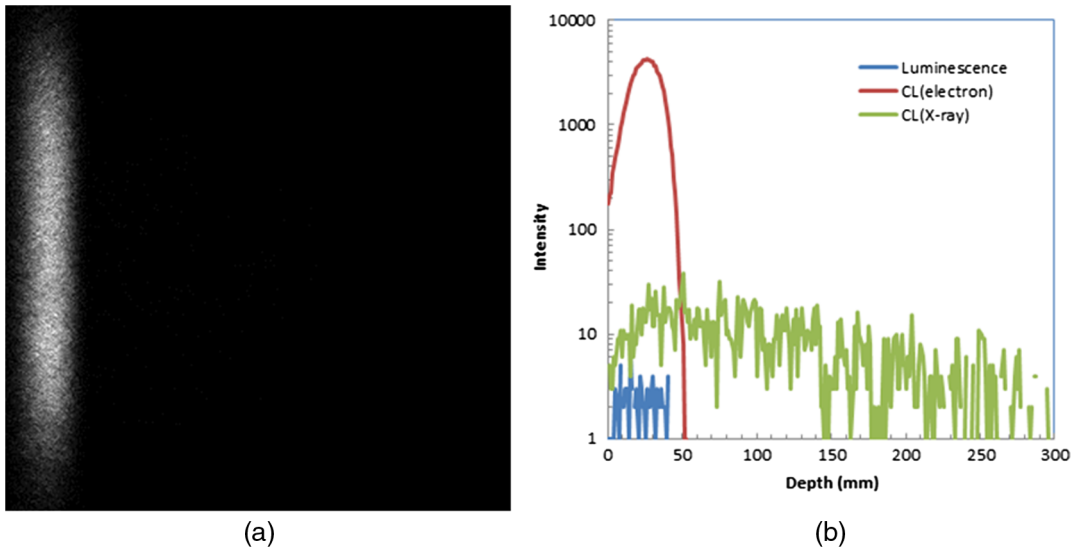
Fig. 7 (a) Simulated image and (b) depth profiles of luminescence and CL for 9-MeV electrons calculated by Monte Carlo simulation.
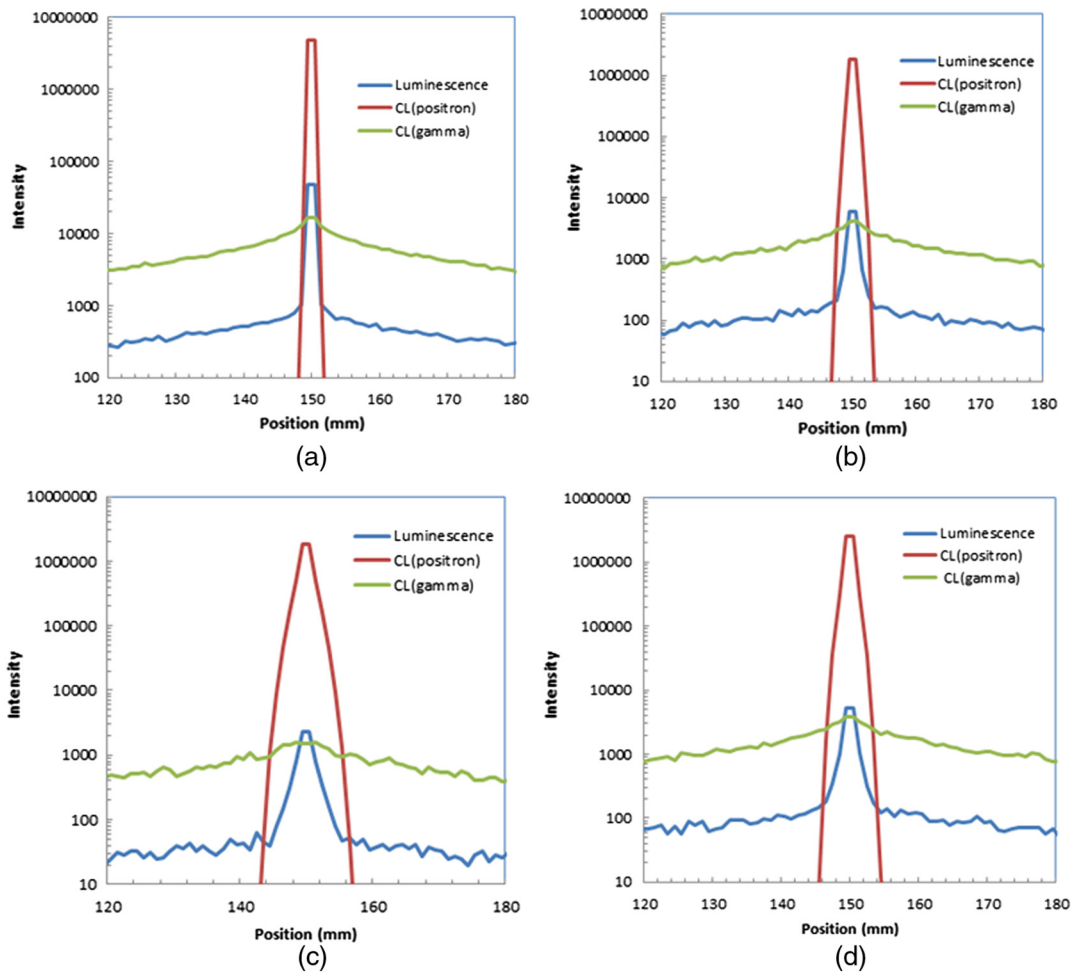
Fig. 8 Simulated depth profiles of luminescence and CL for (a) F-18, (b) C-11, (c) O-15, and (d) N-13 point sources in water calculated by Monte Carlo simulation.
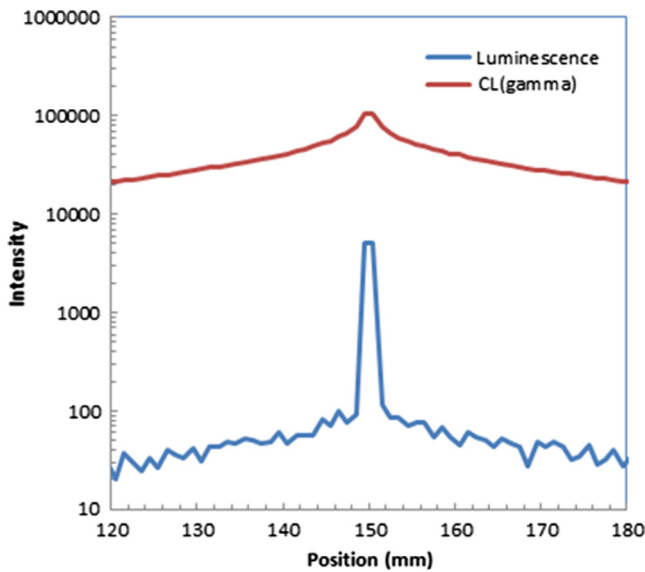
Fig. 9 Simulated depth profiles of luminescence and CL for Co-60 point source in water calculated by Monte Carlo simulation.

Table 1 Luminescence of water and CL fractions calculated by Monte Carlo simulation in all emitted light for protons, carbon ions, x-ray from LINAC, and electrons from LINAC.

	Proton (170 MeV)	Carbon ion (330 MeV)	LINAC x-ray (6 MV)	LINAC electron (9 MeV)
Luminescence of water (%)	33.3	27.1	0.2	0.1
CL				
Total (%)	66.7	72.9	99.8	99.9
Particles (%)	0.4	35.8		
Prompt γ (%)	66.3	37.1		

luminescence of water for protons and carbon ions could be observed at higher contrast as shown in Figs. 4(a) and 5(a).[27] For the depth profile of carbon ions, the CL from the secondary electrons produced by the carbon ions was also observed in the shallow part of the distribution. These CL fractions distorted

the shape of the depth profiles and thus differentiated the depth profiles from the dose distributions. Therefore, some corrections are required for the depth profiles of carbon ions.

The CL for LINAC x-ray and electrons had high intensity and thus was easier to image in a short time.[1–8] However, the angular dependency and nonproportional relation with the energy of electrons also distorted the distribution of the optical images, especially for electrons.[19,33] Accordingly, some corrections of the CL images are also required in the case of CL for LINAC electrons.

For the CL from positrons, no corrections will be required to estimate the dose because positrons are emitted isotropically from the source. Thus, CL from positrons is useful for measuring the distribution and decay curve for the induced positrons by the irradiation of protons or carbon ions.[34,35]

5 Conclusions

We clarified the major components of light photons by the irradiation to water of various types of radiations. For protons, the major fraction of the produced light was the luminescence of water in addition to the CL from the prompt gamma photons produced by the nuclear interactions. For carbon ions, the major fractions of the produced light were the luminescence of water and the CL produced by the secondary electrons of carbon ion in addition to the prompt gamma photons produced by the nuclear interactions. We also confirmed that the major fractions of the produced light from x-ray and electrons from LINAC as well as positrons or high-energy gamma photons were CL. With these results, we confirmed that the major fractions of the produced light from x-ray and electrons from LINAC, positron radionuclides, and Co-60 sources were CL and that the fractions of the luminescence of water were <0.1% to 1.5%.

Disclosures

The authors have no relevant financial interests in this article and no potential conflicts of interest to disclose.

References

1. A. K. Glaser et al., "Projection imaging of photon beams using Cerenkov-excited fluorescence," *Phys. Med. Biol.* **58**(3), 601–619 (2013).
2. R. Zhang et al., "Superficial dosimetry imaging based on Čerenkov emission for external beam radiotherapy with megavoltage x-ray beam," *Med. Phys.* **40**(10), 101914 (2013).
3. J. L. Demers et al., "Cerenkov excited fluorescence tomography using external beam radiation," *Opt. Lett.* **38**(8), 1364–1366 (2013).

Table 2 Luminescence of water and CL fractions in all emitted light for positrons and high-energy gamma photon radionuclides.

	F-18 ($\beta+$) (Max: 0.64 MeV)	C-11 ($\beta+$) (Max: 0.96 MeV)	O-15 ($\beta+$) (Max: 1.70 MeV)	N-13 ($\beta+$) (Max: 1.19 MeV)	Co-60 (γ) (1.17 and 1.33 MeV)
Luminescence of water (%)	1.5	0.7	0.2	0.4	0.4
CL					
Total (%)	98.5	99.3	99.8	99.6	99.6
Positrons (%)	92.4	95.2	98.2	96.8	
511 keV γ (%)	6.1	4.1	1.6	2.8	

4. A. K. Glaser et al., "Three-dimensional Cerenkov tomography of energy deposition from ionizing radiation beams," *Opt. Lett.* **38**(5), 634–636 (2013).
5. A. K. Glaser et al., "Optical dosimetry of radiotherapy beams using Cherenkov radiation: the relationship between light emission and dose," *Phys. Med. Biol.* **59**(14), 3789–3811 (2014).
6. J. Axelsson et al., "Cerenkov emission induced by external beam radiation stimulates molecular fluorescence," *Med. Phys.* **38**(7), 4127–4132 (2011).
7. A. K. Glaser et al., "Projection imaging of photon beams by the Cerenkov effect," *Med. Phys.* **40**(1), 012101 (2013).
8. A. K. Glaser et al., "Time-gated Cherenkov emission spectroscopy from linear accelerator irradiation of tissue phantoms," *Opt. Lett.* **37**(7), 1193–1195 (2012).
9. S. Yamamoto et al., "Optical imaging of water during X-ray beam irradiations from linear accelerator," *Nucl. Instrum. Methods Phys. Res. A* **872**, 174–180 (2017).
10. R. Robertson et al., "Optical imaging of Cerenkov light generation from positron-emitting radiotracers," *Phys. Med. Biol.* **54**, N355–N365 (2009).
11. J. S. Cho et al., "Cerenkov radiation imaging as a method for quantitative measurements of beta particles in a microfluidic chip," *Phys. Med. Biol.* **54**, 6757–6771 (2009).
12. H. Liu et al., "Optical imaging of reporter gene expression using a positron-emission-tomography probe," *J. Biomed. Opt.* **15**, 060505 (2010).
13. A. Ruggiero et al., "Cerenkov luminescence imaging of medical isotopes," *J. Nucl. Med.* **51**, 1123–1130 (2010).
14. J. C. Park et al., "Luminescence imaging using radionuclides: a potential application in molecular imaging," *Nucl. Med. Biol.* **38**(3), 321–329 (2011).
15. Z. Hu et al., "Experimental Cerenkov luminescence tomography of the mouse model with SPECT imaging validation," *Opt Express* **18**, 24441–24450 (2010).
16. S. Yamamoto et al., "Development of a PET/Cerenkov-light hybrid imaging system," *Med. Phys.* **41**(9), 092504 (2014).
17. Y. Xu, H. Liu, and Z. Cheng, "Harnessing the power of radionuclides for optical imaging: Cerenkov luminescence imaging," *J. Nucl. Med.* **52**(12), 2009–2018 (2011).
18. S. Yamamoto et al., "Ultrahigh-resolution Cerenkov-light imaging system for positron radionuclides: potential applications and limitations," *Ann. Nucl. Med.* **28**(10), 961–969 (2014).
19. Y. Helo et al., "Imaging Cerenkov emission as a quality assurance tool in electron radiotherapy," *Phys. Med. Biol.* **59**(8), 1963–1978 (2014).
20. S. Yamamoto et al., "Luminescence imaging of water during proton-beam irradiation for range estimation," *Med. Phys.* **42**(11), 6498–6506 (2015).
21. S. Yamamoto et al., "Luminescence imaging of water during carbon-ion irradiation for range estimation," *Med. Phys.* **43**, 2455–2463 (2016).
22. S. Yamamoto et al., "Luminescence imaging of water during alpha particle irradiation," *Nucl. Instrum. Methods Phys. Res. Sec. A* **819**(21), 6–13 (2016).
23. S. Yamamoto, "Luminescence imaging of water during irradiation of beta particles with energy lower than Cerenkov-light threshold," *IEEE Trans. Radiat. Plasma Med. Sci.* **1**(4), 329–333 (2017).
24. S. Yamamoto et al., "Luminescence imaging of water during irradiation of X-ray photons lower energy than Cerenkov light threshold," *Nucl. Instrum. Methods Phys. Res. A* **832**(1), 264–270 (2016).
25. S. Yamamoto et al., "Stability and linearity of luminescence imaging of water during irradiation of proton-beams and X-ray photons lower energy than the Cerenkov light threshold," *Nucl. Instrum. Methods Phys. Res. A* **883**(1), 48–56 (2018).
26. T. Yabe et al., "Estimation and correction of produced light from prompt gamma photons on luminescence imaging of water for proton therapy dosimetry," *Phys. Med. Biol.* **63**, 04NT02 (2018).
27. T. Yabe et al., "Addition of luminescence process in Monte Carlo simulation to precisely estimate the emitted light from water during proton and carbon-ion irradiations," *Phys. Med. Biol.* **63**(12), 125019 (2018).
28. K. W. Jang et al., "Fiber-optic Cerenkov radiation sensor for proton therapy dosimetry," *Opt. Express* **20**(13), 13907–13914 (2012).
29. A. Darafsheh et al., "The visible signal responsible for proton therapy dosimetry using bare optical fibers is not Čerenkov radiation," *Med. Phys.* **43**(11), 5973–5980 (2016).
30. S. Yamamoto et al., "Source of luminescence of water lower energy than the Cerenkov-light threshold during irradiation of carbon-ion," *J. Phys. Commun.* **2**, 065010 (2018).
31. W. Brian et al., "Maps of in vivo oxygen pressure with submillimetre resolution and nanomolar sensitivity enabled by Cherenkov-excited luminescence scanned imaging," *Nat. Biomed. Eng.* **2**(4), 254–264 (2018).
32. S. Agostinelli et al., "GEANT4: a simulation toolkit," *Nucl. Instrum. Methods A* **506**, 250–303 (2003).
33. S. Yamamoto et al., "Imaging of produced light in water during high energy electron beam irradiations from a medical linear accelerator," *Radiat. Meas.* **116**, 1–9 (2018).
34. S. Yamamoto et al., "High resolution Cerenkov light imaging of induced positron distribution in proton therapy," *Med. Phys.* **41**, 111913 (2014).
35. T. Masuda et al., "Measurement of nuclear reaction cross sections by using Cherenkov radiation toward high-precision proton therapy," *Sci. Rep.* **8**(1), 2570 (2018).

Yoshiyuki Hirano: Biography is not available.

Seiichi Yamamoto is a professor at the Graduate School of Medicine, Nagoya University. His research interests are developing new imaging systems such as PET, SPECT, and optical, as well as hybrid imaging systems. Recently, he discovered a new phenomenon, "luminescence of water during radiation irradiation lower energy than Cerenkov-light threshold" and he is extensively exploring the new light.